LAWRENCE
LIVERMORE
NATIONAL
LABORATORY

UCRL-CONF-221713

Mitigating atmospheric effects in high-resolution infra-red surveillance imagery with bispectral speckle imaging

C. J. Carrano

May 30, 2006

SPIE International Symposium on Optics and Photonics,
Image Reconstruction from Incomplete Data IV
San Diego, CA, United States
August 13, 2006 through August 17, 2006

Mitigating atmospheric effects in high-resolution infra-red surveillance imagery with bispectral speckle imaging

C. J. Carrano
Lawrence Livermore National Laboratory (LLNL), 7000 East Avenue, Livermore, CA 94550

ABSTRACT

Obtaining a high-resolution image of an object or scene from a long distance away can be very problematic, even with the best optical system. This is because atmospheric blurring and distortion will limit the resolution and contrast of high-resolution imaging systems with substantial sized apertures over horizontal and slant paths. Much of the horizontal and slant-path surveillance imagery we have previously collected and successfully enhanced has been collected at visible wavelengths where atmospheric effects are the strongest. Imaging at longer wavelengths has the benefit of seeing through obscurants or even at night, but even though the atmospheric effects are noticeably reduced, they are nevertheless present, especially near the ground. This paper will describe our recent work on enhanced infra-red (IR) surveillance using bispectral speckle imaging. Bispectral speckle imaging in this context is an image post-processing algorithm that aims to solve the atmospheric blurring and distortion problem of imaging through horizontal or slant path turbulence. A review of the algorithm as well as descriptions of the IR camera and optical systems used in our data collections will be given. Examples of horizontal and slant-path imagery before and after speckle processing will also be presented to demonstrate the resolution improvement gained by the processing. Comparisons of IR imagery to visible wavelength imagery of the same target under the same conditions will be shown to demonstrate the tradeoffs of going to longer wavelengths.

1.0 INTRODUCTION

For many surveillance and target identification applications the imaging system must look through the atmosphere along a horizontal or slant path. Turbulence along the path causes variations in the index-of-refraction that lead to phase errors in the propagating field. When the optical beam is brought to focus the resulting image is blurred and warped by the atmospheric phase errors. For a typical near-ground horizontal path the blurring can be quite severe. The resolution of a substantial sized telescope (> several cm aperture) can be reduced by an order of magnitude or more along a few kilometer horizontal path in average to strong atmospheric turbulence.

In a short exposure image obtained through the atmosphere, the atmospheric phase errors are frozen in time. The image contains spatial frequencies all the way out to the diffraction limit. But, if the short exposure images are averaged, the resulting long exposure image is blurred. The high spatial frequencies are lost in the averaging process. If we record a series of short exposure images, we can use bispectral speckle image processing algorithms to recover the correct image phases and produce a high-resolution image. The algorithm[1,2,3] averages the bispectrum of the image. This average has the property that the random atmospheric phase errors average out leaving the bispectrum of the object itself. The image phase can be reconstructed using a three-point recursive spatial integration algorithm. Our specific modifications to handle the more complex surveillance imaging situations including anisoplanatism and extended scenery are discussed in Ref. 4.

We have demonstrated via many experiments the usefulness of sub-field bispectral speckle image processing to compensate atmospheric blurring effects. Most of our previous work in enhanced surveillance speckle imaging was performed at visible wavelengths[4,5,6,7,8]. We now investigate and report on speckle imaging at longer wavelengths. Infra-red (IR) imaging provides a number of benefits compared to visible imaging and consequently is a mainstay of many tactical surveillance and targeting systems. We already know that IR imaging can be performed day or night, and even see through obscurants. However, it will also extend the range and/or turbulence strengths over which high-resolution imagery, raw or speckle processed, may be obtained compared to visible wavelengths. This is because atmospheric turbulence has a smaller effect on images at longer wavelengths, therefore, more turbulence and/or longer ranges can be accommodated. This is because the atmospheric coherence length (r_0) and the isoplanatic angle (θ_0) both scale with $\lambda^{6/5}$, whereas the diffraction limit scales linearly with wavelength[9].

You may address correspondence to Carmen Carrano, cjc@llnl.gov

2.0 NEAR INFRA-RED (NIR) IMAGING

The first IR camera system we used for data collection was a near-IR system. We describe the system and show results in this section.

2.1 System description

The imaging system consisted of several key components which are listed below:

- Celestron, 8-inch, f/10, Schmidt-Cassegrain telescope
- 3x Barlow lens to increase magnification to 5 urad/pixel
- Indigo Phoenix NIR camera (320x256 pixels, 0.9-1.7 um spectral band, 30 um pixel pitch)
- Data acquisition computer

A photograph of the setup is shown in Figure 1. We transported the system to a location onsite at LLNL that had a clear view of the Livermore waste disposal site and surrounding hillsides which are approximately 7-8 km distant. We expected to find vehicles and other interesting objects to image, which was certainly the case. Figure 2 shows a wide-field photograph of our imaging target region from our data collection site.

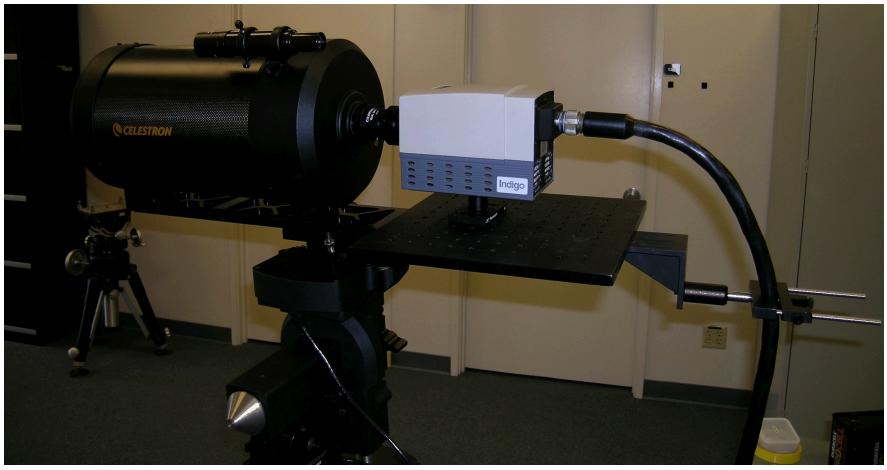

Figure 1: Photograph of NIR camera attached to Celestron telescope.

Figure 2: Photograph of target area roughly 7-8 km range from camera location at LLNL.

2.2 NIR Imagery and processed results

We now show a selection of results from our NIR data collected in January-February, 2005.

2.2.1 Person

The first result we show is that of a person imaged from roughly 0.4 kilometers away over a pure horizontal path in Figure 3. The weather was cool and calm on this winter morning. While the image quality of the sample frames does not prevent us from reading the letters or knowing there is a person standing there, the speckle processed image allows us to clearly see the facial details of the person and exhibits sharp edges on the letters. The grayscale shading in terms of object coloring can be misleading in IR wavelengths as the person was actually wearing a black hat and a black shirt and has dark hair, but nevertheless, the speckle processing results in high-resolution, high-contrast imagery.

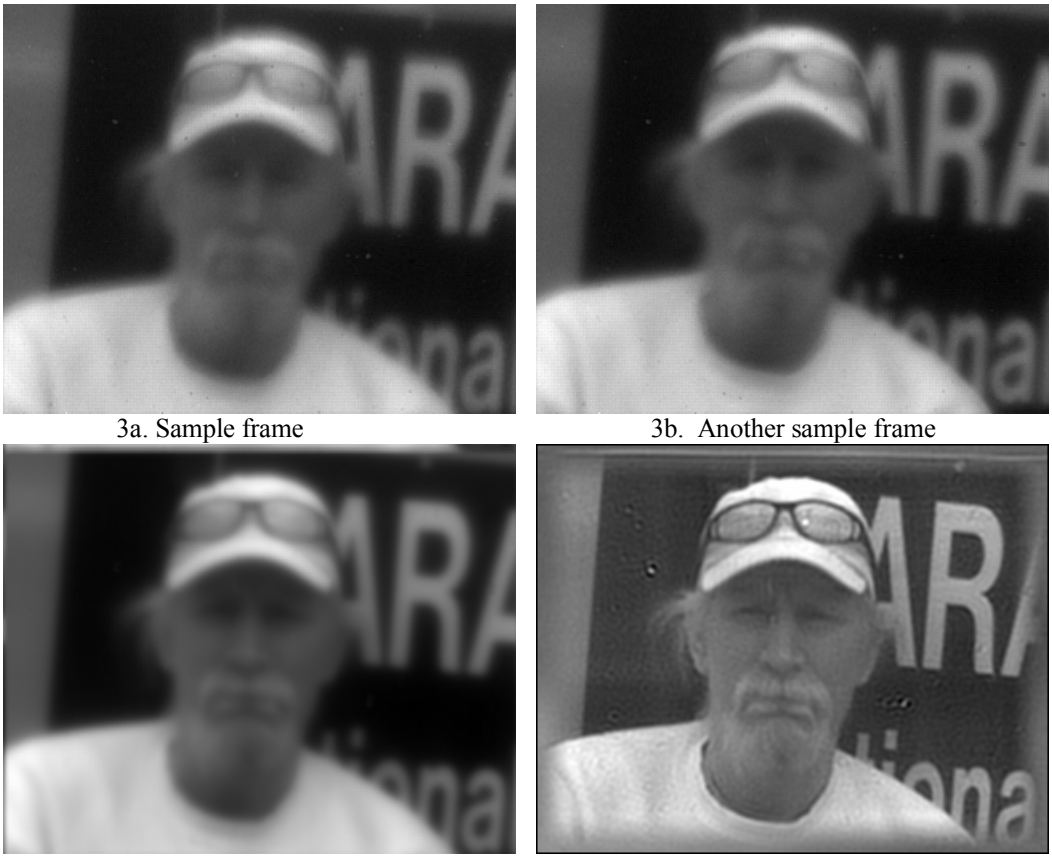

3a. Sample frame 3b. Another sample frame

3c. Shift-and-add 100 frames 3d. Speckle processed

Figure 3: Face of person imaged through a 20 cm diameter telescope at roughly half a kilometer range in the NIR before and after speckle processing.

2.2.2 Objects at 8 km range

The results we show in this section are of vehicles along with various objects such as signs, posts, foliage, and debris at roughly 8 km range over a slightly upward looking slant path (see Figure 2). Figure 4 shows a tractor and a "ONE WAY" sign. In the speckle processed image, the sign is more clearly readable and the tractor more identifiable. In fact, when we were acquiring the imagery, we did not even know that we were looking at a vehicle until after it was speckle processed. Figure 5 shows what is probably a storage container surrounded by debris. In the speckle processed image,

everything is much higher resolution revealing greater details about the debris content. This is also evident if we look at the frequency content in a small region of the debris shown in Figure 6.

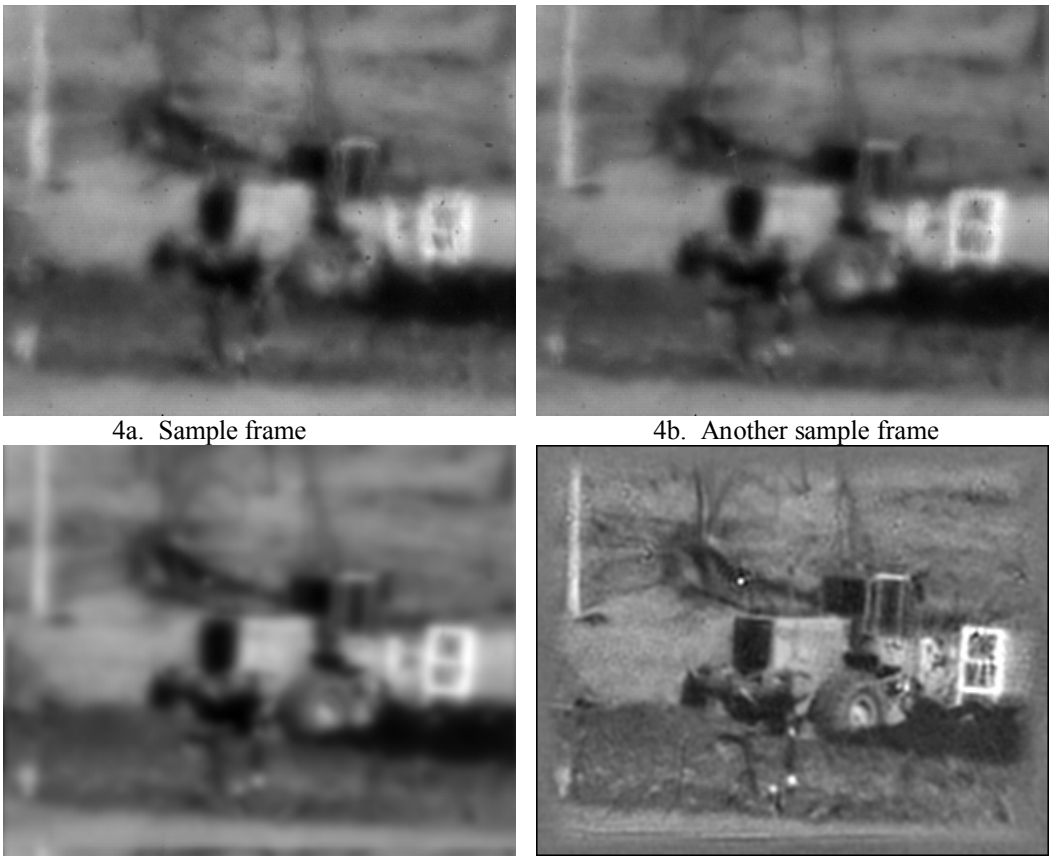

4a. Sample frame

4b. Another sample frame

4c. Shift-and-add 100 frames

4d. Speckle processed

Figure 4: Tractor and sign at the Livermore dump imaged from 8 km away before and after speckle processing.

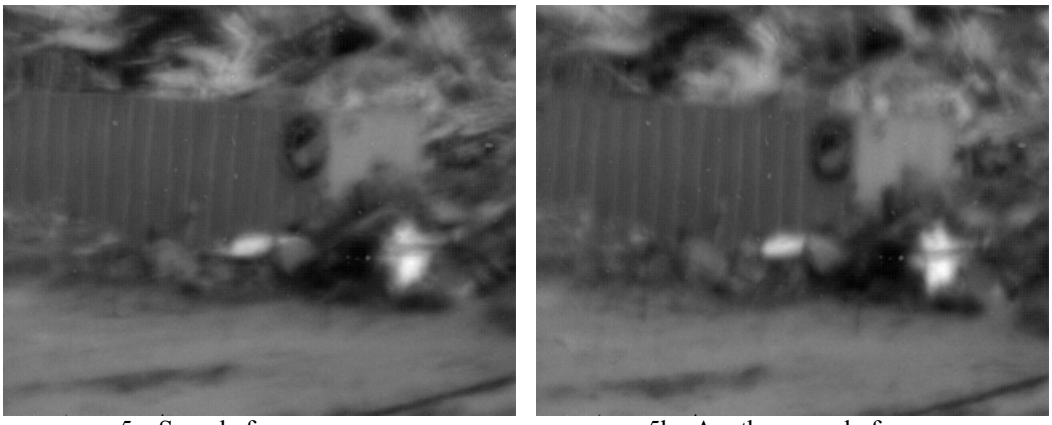

5a. Sample frame

5b. Another sample frame

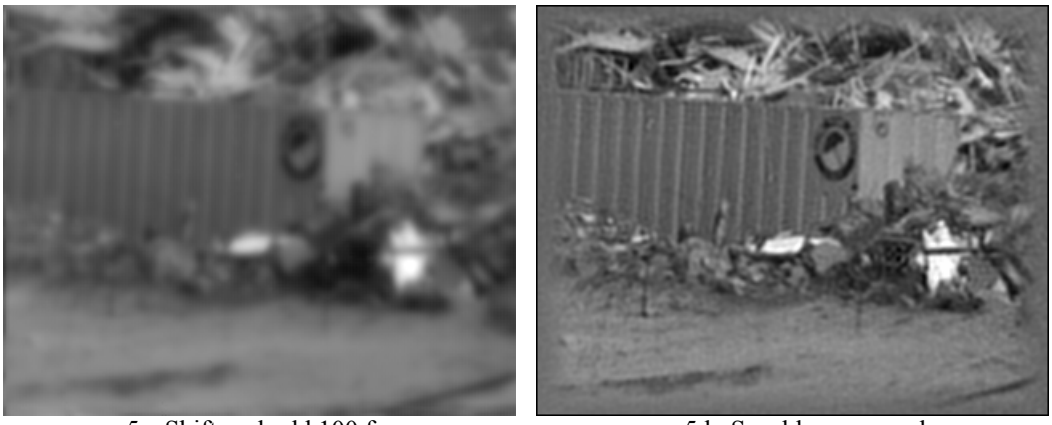

5c. Shift-and-add 100 frames 5d. Speckle processed

Figure 5: Storage container and debris at the Livermore dump imaged from 8 km range before and after speckle processing.

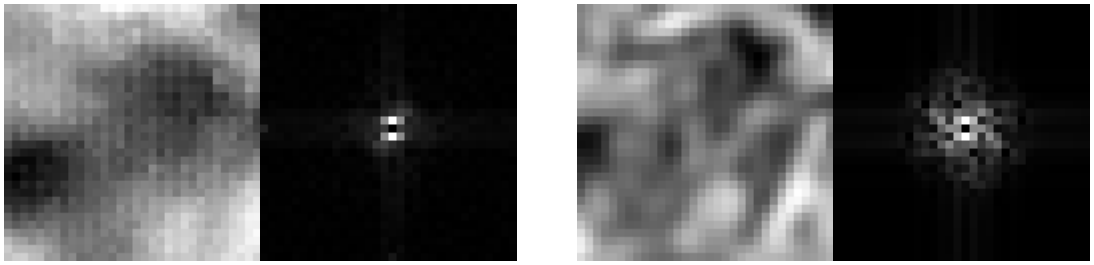

Small region of raw frame and its spectrum Small region of processed image and its spectrum

Figure 6: Magnified small regions of imagery and the magnitude of their Fourier transforms before and after speckle processing revealing lower noise and much higher resolution.

3.0 MID-WAVE IR (MWIR) IMAGING

The second IR camera system we used for data collection was an MWIR system. We describe the system and show results in this section.

3.1 System description

The transition from NIR to MWIR was not as simple as swapping cameras. The Schmidt-Cassegrain telescope used for all the visible and NIR experiments was useless in the MWIR because the corrector plate is made of a material opaque to the 3-5 um band. As a result, employment of a new optical setup with all reflective optics was necessary. A photograph of the all reflective optic imaging setup is shown in Figure 7.
The imaging system consisted of several key components which are listed below:

- STARHOC, 8-inch, f/4, Newtonian reflector telescope
- Indigo Phoenix MWIR camera (320x256 pixels, 3.0-5.0 um spectral band, 30 um pixel pitch). Exposure time fixed at 2.3 ms. Frame rate > 100 Hz.
- Unable to use Barlow lens, so sampling is 37.5 urad/pixel
- Data acquisition computer

Figure 7: Newtonian reflector telescope with Indigo camera attached and looking out the (open) window of our observation location.

3.2 Imagery and processed results

We now show a selection of results from our MWIR data collection in May, 2005. The weather during the data collection was near 90 degrees F, which means that we expect stronger turbulence conditions than the NIR data collection described previously. Arrows drawn on the picture in Figure 8 indicate the physical locations of the imagery that we will show in the next two subsections.

Figure 8: View from our observation location in May 2005. Arrows indicate the target locations for imagery shown in this report.

3.2.1 House on a hill at 9 km range

This first result we show in Figure 9 is that of a house (and surrounding foliage) on top of a hill, roughly 1100 feet above the ground level and 9 km distant from the observing site. The first thing we notice about this MWIR raw imagery is that the raw frames are not overly blurry. The dominant effect here is warping and waviness, which is more evident when watching a movie of the frames. The lower degree of blurriness is due to the under-sampling of the aperture; we are under-sampling the Nyquist frequency for the aperture size at 4 um by a factor of 3.75. However, the speckle processed image doesn't have any of the waviness of the raw imagery and is much sharper than either the raw imagery or the shift-and-add image.

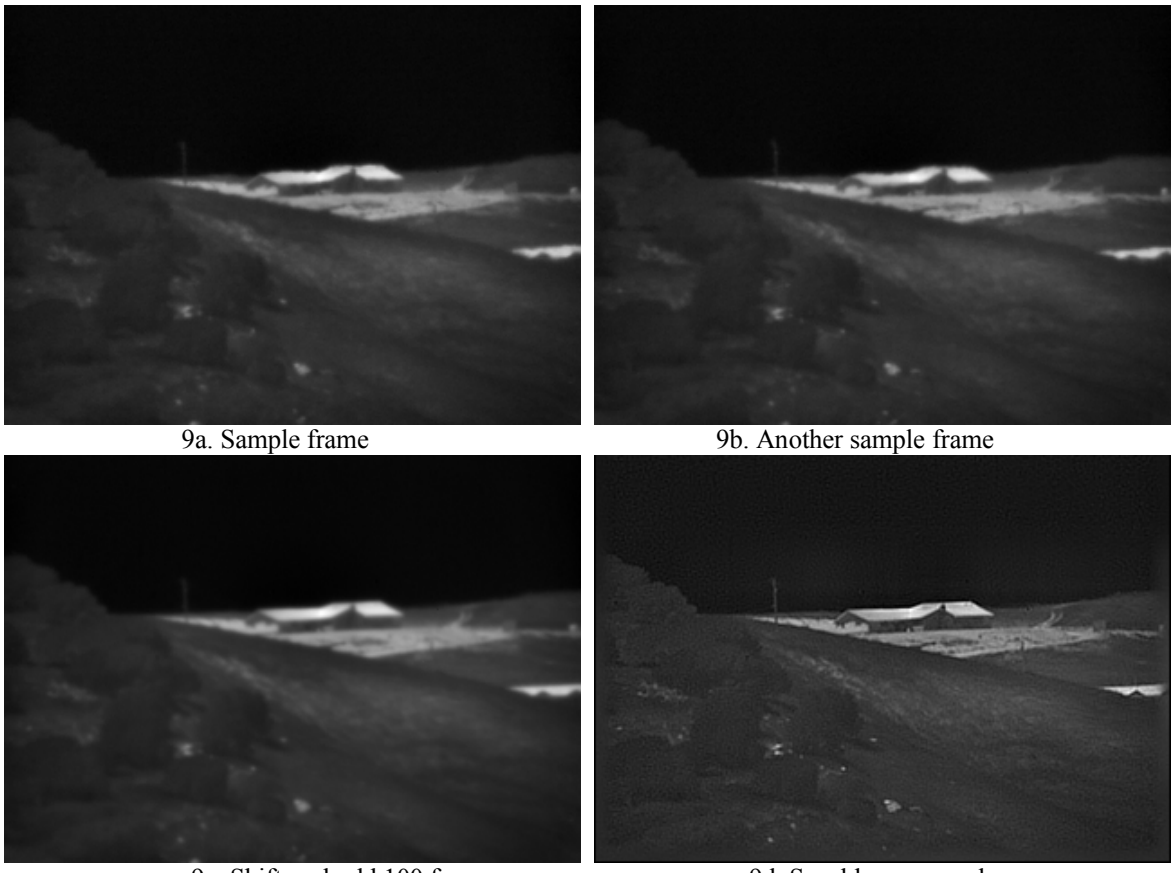

9a. Sample frame

9b. Another sample frame

9c. Shift-and-add 100 frames

9d. Speckle processed

Figure 9: Image of a house on top of a hill at roughly 9 km range.

3.2.2 Objects at 6 km

For this next case shown in Figure 10, we pointed the telescope as close to horizontal as we could in search of stronger turbulence. As we can see, foreground trees block much of the path, limiting our ability to go purely horizontal over a long distance. But by decreasing our slant angle by just over a factor of two, we noticed a significant increase in turbulence on the camera monitor during the experiment. Imagery from higher on the hill on that same day was processed with an r_0 of 1.7-2.0 cm, while this dataset necessitated a lower r_0 of 1.5 cm, indicating stronger turbulence.

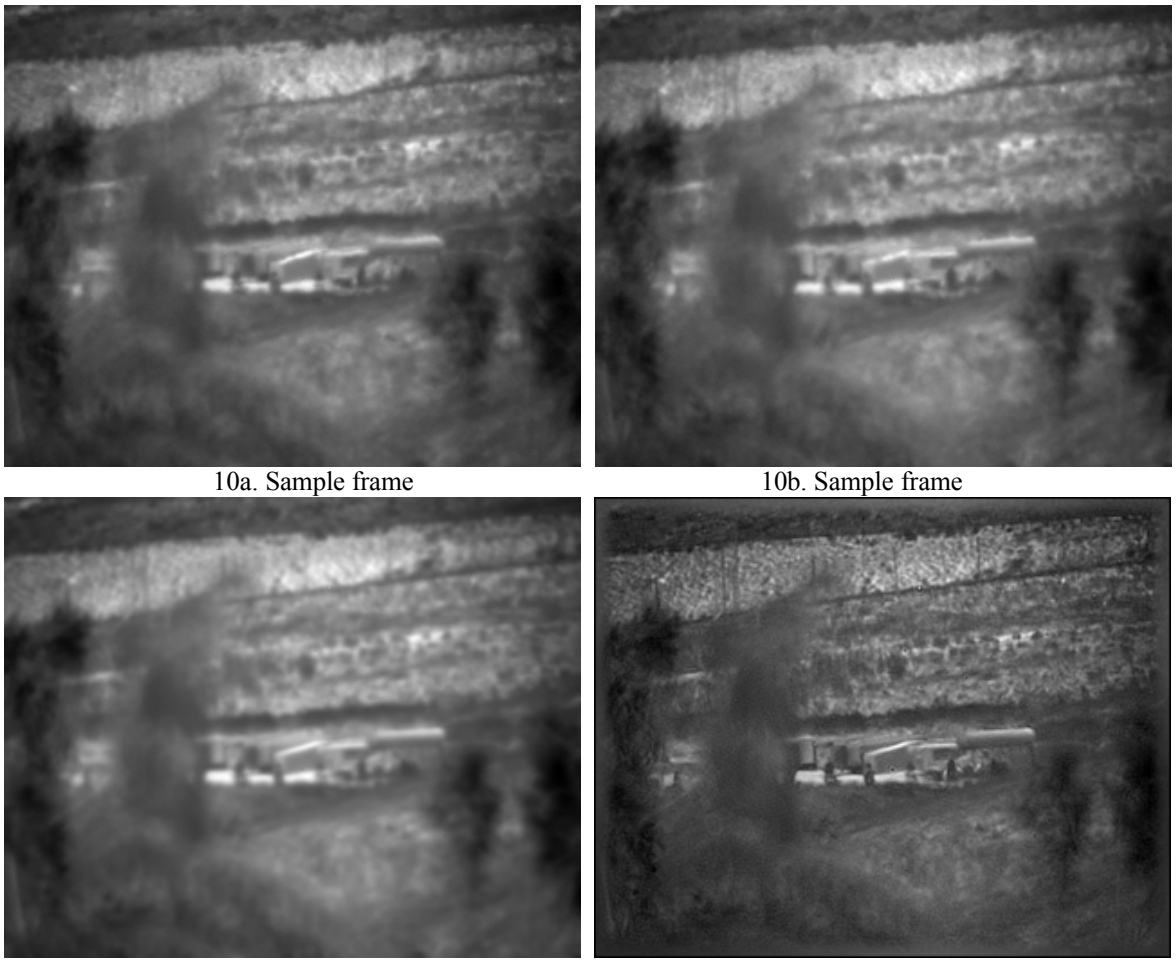

10a. Sample frame 10b. Sample frame

10c. Shift-and-add 100 frames 10d. Speckle processed

Figure 10: Objects and surrounding foliage at roughly 6 km range.

4.0 COMPARISON BETWEEN SPECTRAL BANDS

4.1. NIR versus Visible

In Figure 11 we show a comparison between imagery of the same target acquired at nearly the same time with the NIR camera and a visible light camera on a nice winter day. The visible images have been rescaled to have the same sampling interval as the NIR images for easier comparison. In both cases we are using the 3x Barlow lens, giving a sampling interval in the visible of 1.12 urad/pixel and 5 urad/pixel in the NIR. Two obvious differences are noticeable in the raw shift-and-add images. The first is that the resolution of the visible case is slightly lower. We can see this by looking at certain small features in the visible image that are almost completely blurred out while they are still observable in the NIR image. The other difference is the contrast and appearance of the scenery owing to the varying reflectivity of different materials as a function of wavelength. For this particular scene, the NIR imagery has more pleasing contrast with better signal to noise ratio. Another way to visualize the raw data is by looking at the short exposure time-averaged power-spectra at both wavelengths. On the left side of Figure 12 we see the visible power-spectrum energy falls into the noise below $0.3(D/\lambda)$'s or diffraction limits, while on the right side of Figure 12 we see the NIR power-spectrum energy is good all the way out to the edge of it's spectrum (i.e. ~.55 (D/λ)'s). Indications from this plot are that if we had a longer focal length optic, it is possible that we could have obtained even better NIR resolution, since we were under-sampling the diffraction limit. The speckle processed results in the NIR appear to have slightly better processed resolution and with far less artifacts than in the visible.

What we learn is that for this 8 km slant path, under these atmospheric and sampling conditions, we are better off to image in the NIR if we want artifact free high-resolution images. Though, it is conceivable we could obtain improved visible results than shown here with a different CCD camera with higher sensitivity and/or lower noise.

Visible wavelength – down-sampled to NIR sample interval (below)

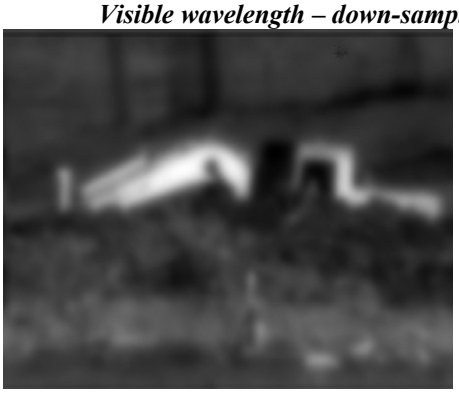

11a. Shift and add 100 frames

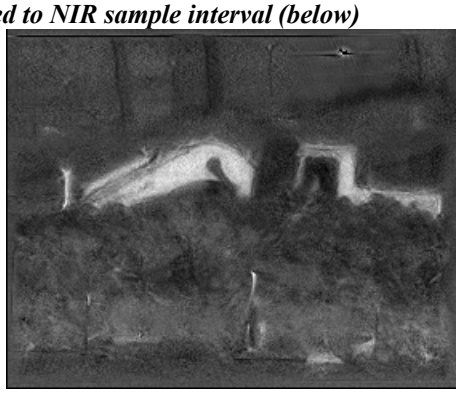

11b. Speckle processed with r0 = 0.8 cm

NIR wavelength (below)

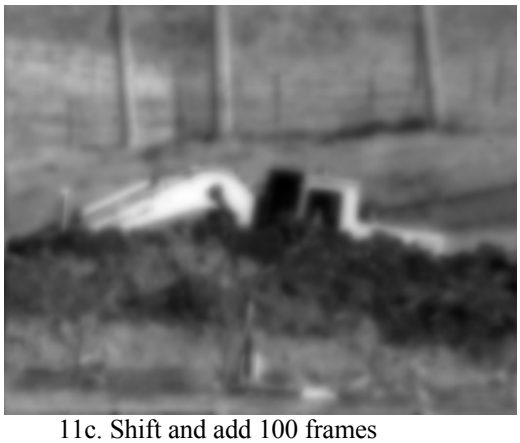

11c. Shift and add 100 frames

11d. Speckle processed with r0 = 1.5 cm

Figure 11: Comparison of visible and NIR imagery of same target at 8 km range taken at nearly the same time.

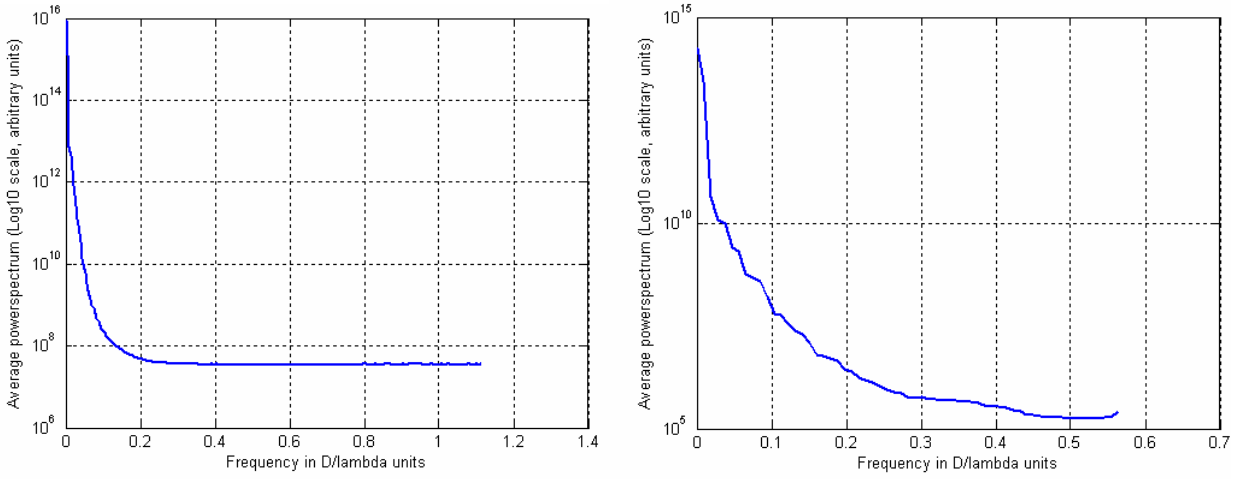

Figure 12: Comparison of 100 frame radial averaged power-spectra of visible (left) and NIR (right) section of imagery from unprocessed datasets in Figure 12. The x-axis is in diffraction limit (D/λ) units. The y-axis is a log scale.

4.2 MWIR versus Visible

In comparing visible to MWIR, we must realize that the diffraction limit at these two wavelengths is nearly an order of magnitude different for the same aperture size. The diffraction limit of a 20 cm optic at 0.5 um is 2.5 μrad while at 4 um, it is 20 μrad. Also, the actual angular pixel sizes of each wavelength case used for the experiment are quite different owing to the differing physical pixel sizes. In the visible setup, the camera is sampling at 8.375 μrad/pixel with no Barlow lens, while for the MWIR setup with the same telescope, the camera is sampling at 37.5 μrad/pixel. Figure 13 shows shift-and-add as well as the speckle processed results for the two wavelengths. The visible images are shown down-sampled to the IR image pixel size for comparison and what we see is nice reconstructions in both wavebands at those sample intervals. In looking at the visible imagery at full scale, such as in Figure 14, we find that there is not much additional information available, because the atmospheric turbulence is so strong here (i.e. the processing required millimeter-scale r_0 in the visible).

As in the last sub-section, another way to visualize this is by looking at the short exposure time-averaged power-spectra at both wavelengths. On the left side of Figure 15 we see the visible power-spectrum energy falls into the noise below 0.3(D/λ)'s or diffraction limits, while on the right side of Figure 15 we see the MWIR power-spectrum energy is good all the way out to the edge of it's spectrum (i.e. .25 (D/λ)'s). It is clear from the MWIR plot that if we had a longer focal length telescope, we could have obtained even better MWIR resolution, since the camera was well under-sampling the diffraction limit in the MWIR. Though substantial improvement in resolution is found by speckle processing the visible case, we see that the resolution advantage normally attributed the visible wavelength imaging is not the case in these conditions and the resolution is reduced to nearly that of the MWIR system. In addition, imaging in the MWIR gives nice contrast in much of the scene, such as the foliage, which is less observable in the visible, while other features are more observable in the visible, such as the fence posts.

5.0 CONCLUSIONS AND FUTURE

We have demonstrated significant resolution improvement and distortion mitigation of long range IR imagery with the use of bispectral speckle imaging. We have also demonstrated that employing longer wavelengths can be advantageous to shorter wavelengths both from a signal to noise standpoint and an overall image contrast standpoint in average to strong turbulence. The potential for improved long distance horizontal or slant-path imagery in any waveband from the visible through the IR with the use of bispectral speckle imaging is important for enabling an expanded range of surveillance applications.

An important point to mention about speckle imaging is that, although it is computationally intensive, it can be run quite fast, especially on smaller sized imagery. On a standard desktop PC (2-3 Ghz), using un-optimized code, 30 frames of 256x256 pixel data can be processed in about a second, which means that video-rate speckle processing is obtainable with some software optimization and possibly some special purpose hardware for larger arrays. In a future paper, I will discuss the modifications that we have made to our speckle processing capability so that it may operate in a continuously updating fashion, allowing for actual atmospherically compensated video to be generated.

ACKNOWLEDGEMENTS

I would like to acknowledge the help of Jack Tucker and Richard Combs for their help with the IR optical system setups and data collections, and Darron Nielsen for the use of his MWIR camera.
Work performed under the auspices of the U.S. Department of Energy by UC, Lawrence Livermore National Laboratory under contract No. W-7405-ENG-48.

MWIR wavelength (below)

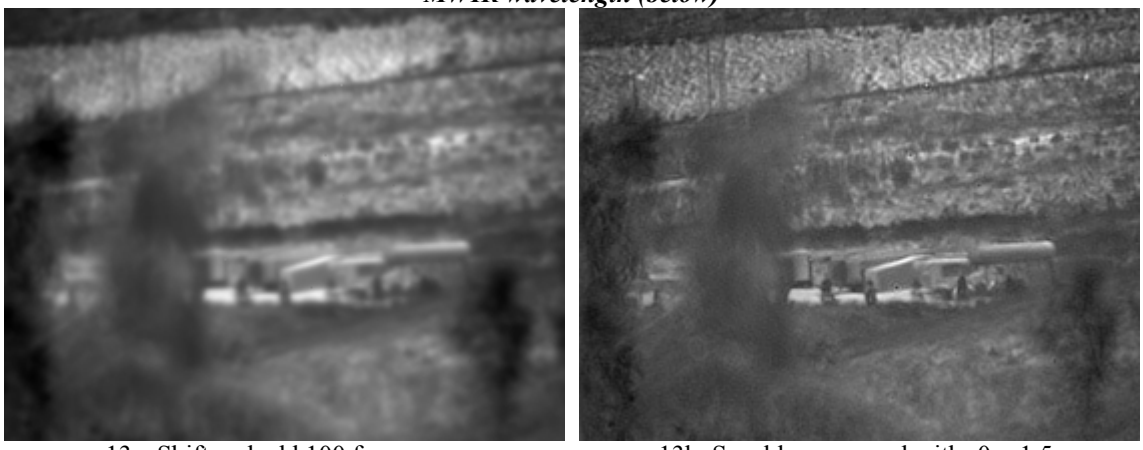

13a. Shift and add 100 frames

13b. Speckle processed with r0 = 1.5 cm

Visible wavelength – down-sampled to MWIR sampling interval (below)

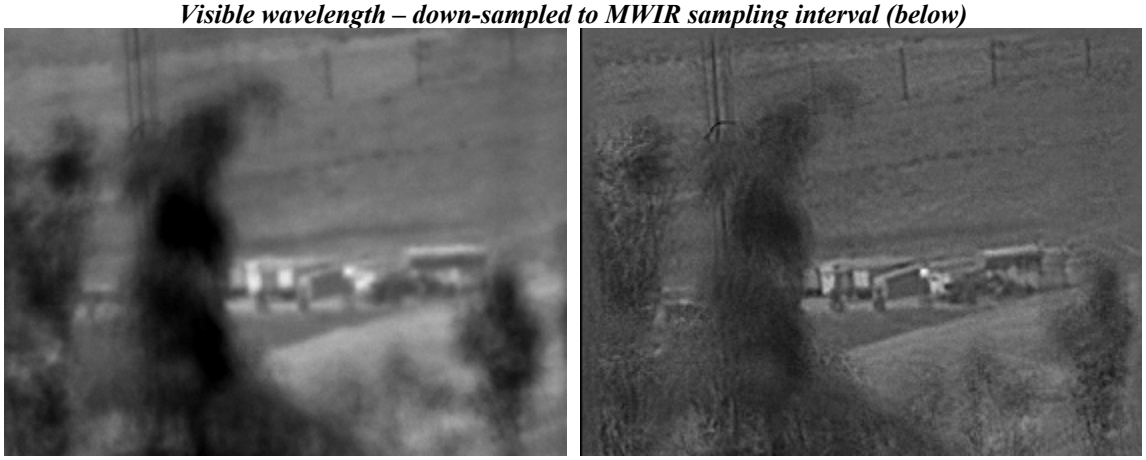

13c. Shift and add 100 frames

13d. Speckle processed with r0 = 1.5 mm

Figure 13: Comparison of visible and MWIR imagery of same target at 6 km range taken at nearly the same time.

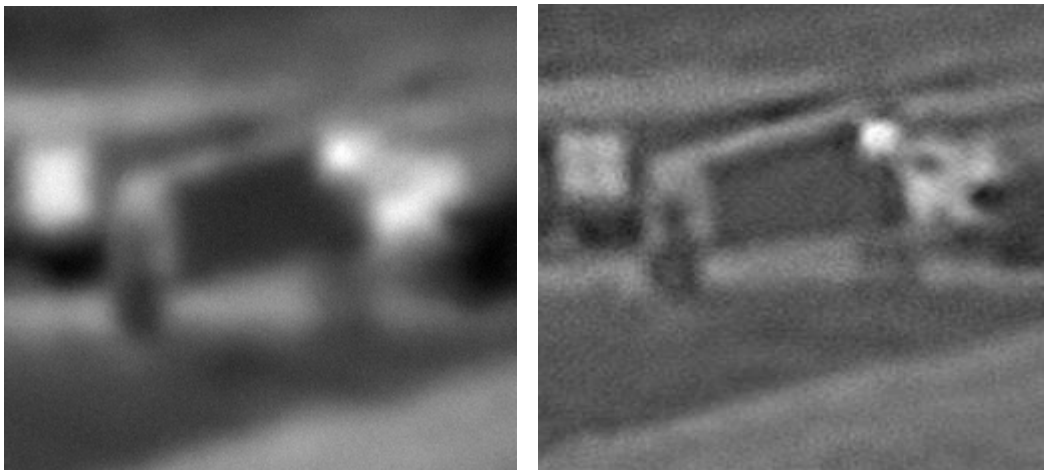

Figure 14: Small region of visible imagery at full size before (left) and after (right) speckle processing.

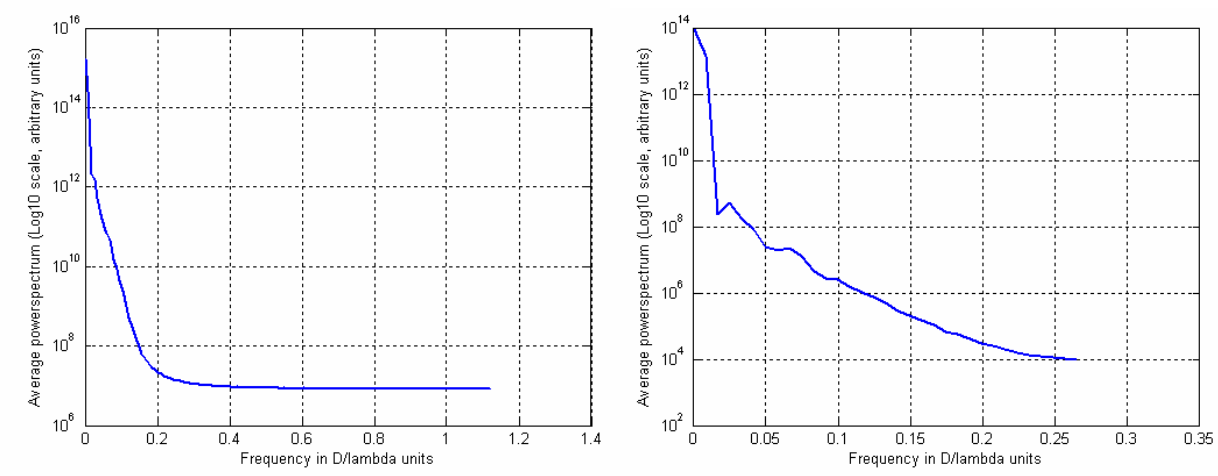

Visible power-spectrum MWIR power-spectrum

Figure 15: Comparison of 100-frame radial averaged power-spectra of visible and MWIR section of raw imagery from datasets in Figure 13. The x-axis is in diffraction limit or D/λ units. D is 20 cm, and the λ's are 0.5 μm and 4.0 μm respectively. The y-axis is on a log scale.

REFERENCES

1. A.W. Lohmann, G. Weigelt, and B. Wirnitzer. "Speckle masking in astronomy: triple correlation theory and applications", Applied Optics, Vol 22, pp. 4028 (1983).
2. T. Lawrence, D. Goodman, E. Johansson, "Speckle Imaging of satellites at the U.S. Air Force Maui Optical Station", Applied Optics, Vol 31, No 29, (1992).
3. T. W. Lawrence, J.P. Fitch , D. M. Goodman, N. A. Massie, R. J. Sherwood, and E. M. Johansson, "Extended image reconstruction through horizontal path turbulence using bispectral speckle interferometry," Opt. Eng. **32**, pp. 627-636 (1992)
4. C. J. Carrano, "Speckle Imaging over Horizontal Paths", Proceedings of the SPIE -High Resolution Wavefront Control: Methods, Devices, and Applications IV, 4825, pp. 109-120, (2002)
5. C. J. Carrano, J. M. Brase, "Horizontal and Slant Path Surveillance with Speckle Imaging", AMOS Technical Conference Proceedings, (2002)
6. C. J. Carrano, "Progress in horizontal and slant-path imaging using speckle imaging", Proceedings of the SPIE-LASE2003 - Optical Engineering at the Lawrence Livermore National Laboratory, **5001** (2003) pp. 56-64
7. C. J. Carrano, "Anisoplanatic performance of horizontal-path speckle imaging", Proceedings of the SPIE, **5162** (2003)
8. C. J. Carrano, J. M. Brase. "Adapting high-resolution speckle imaging to moving targets and platforms", Proc. SPIE, **5409** (2004)
9. J. Hardy, Adaptive Optics for Astronomical Telescopes, Oxford Press, 1998, pp 92